Geophys. J. Int. (2003) **155,** 327–339

Wavefield extrapolation and amplitude-variation-with-angle migration in highly discontinuous media

Jianfeng Zhang* and Kees Wapenaar

Centre for Technical Geoscience, Delft University of Technology, PO Box 5028, 2600 *GA Delft, the Netherlands. E-mail: C.P.A.Wapenaar@ctg.tudelft.nl*

Accepted 2003 May 26. Received 2003 May 26; in original form 2002 February 25

SUMMARY

Current macromodel-based one-way wavefield extrapolation ignores the practical highly discontinuous character of rock formations. The main effects of this highly discontinuous behaviour on transmitted wavefields are angle-dependent dispersion and amplitude losses. In this paper the angle-dependent dispersion and amplitude losses are quantified by a proposed extended macro model, which is closely related to the current macro model except that two stochastic parameters on the rock formations are added. The stochastic parameters are derived based on the observation of power-law behaviour of subsurface heterogeneity. The resulting replacement medium described by the extended macro model is an anisotropic medium with anelastic losses. Explicit extrapolation operators are used to perform forward and inverse wavefield extrapolation in the inhomogeneous replacement medium, which mimics a true subsurface that is moderately inhomogeneous at the macro scale and highly discontinuous at the subwavelength scale. The stability of the inverse wavefield extrapolation is achieved through controlling the maximum angle of propagation. Also a table-driven true-amplitude pre-stack migration scheme is proposed, which can approximately eliminate the dispersion effects of the fine-layering together with the geometrical spreading effects in imaging the subsurface based on the extended macro model. A number of numerical examples are presented to illustrate the algorithms.

Key words: AVA, fine-layering scattering, migration.

INTRODUCTION

The main process in seismic migration is the elimination of propagation effects from the seismic measurements. Usually these propagation effects are quantified by a macro model, which contains the main geological boundaries in the subsurface and the average velocities between these boundaries. However, the rock formations as revealed by well logs and core samples are highly discontinuous at all length-scales down to a few centimetres and smaller. Extensive studies on wave propagation through (1-D) finely layered media (e.g. O'Doherty & Anstey 1971; Schoenberger & Levin 1979) have shown that short-period internal multiples may seriously affect the apparent propagation properties of the seismic wavefield. The main effects are angle-dependent dispersion and amplitude losses of the transmitted wavefield. It is obvious that the macro model does not include the details of rock formations at such small scales. Hence, the seismic processing based on the macro model will not compensate for these angle-dependent dispersions and amplitude losses. This may result in dispersed images and erroneous amplitude-variation-with-angle (AVA) effects. It is not realistic to attempt to construct a velocity model that includes the correct details of the rock formations. Instead, it is more feasible to describe the changes of the primary wave due to the fine-layering scattering (i.e. short-period internal multiples) in terms of the stochastic wave propagation and then use the stochastic parameters that characterize the medium to mimic the apparent propagation properties of wavefield. This approach was followed by O'Doherty & Anstey (1971) and Banik *et al.* (1985) for normal incident wavefields through 1-D acoustic media, by Shapiro & Zien (1993) for obliquely incident wavefields through 1-D acoustic media, and by Burridge & Chang (1989) for obliquely incident wavefields through 1-D elastic media. Hermann & Wapenaar (1992) and Wapenaar *et al.* (1994) introduced an extended macro model. The extended macro model aims to replace a finely layered medium by a homogeneous anisotropic medium with anelastic losses in such a way that the transmission response of this replacement medium is effectively the same as the transmission response of the original finely layered medium. This provides a possibility to take the fine-layering scattering into account in seismic processing for a practical subsurface that is moderately inhomogeneous at the macro scale and highly discontinuous at the subwavelength scale.

In this paper, we further develop the idea of the extended macro model. Instead of describing the model with frequency-dependent

*On leave from: The Department of Engineering Mechanics, Dalian University of Technology, Dalian 116023, China. E-mail: zhangjf@mail.igcas.ac.cn

vertical and horizontal complex phase velocities as introduced in Wapenaar *et al.* (1994), we directly derive the dispersion relation for the replacement medium based on the apparent transmission response of the original finely layered medium, and then define the average velocities and stochastic parameters as those used by Wapenaar *et al.* (1994) as a new parametrized extended macro model. This means that the proposed replacement model has a less severe angle limitation for mimicking the wave propagation in the true finely layered medium and it is able to handle fine-layering structures that are either horizontal or tilted. Also, in the proposed method the Kramers–Kronig relations are satisfied for all propagation angles. By developing phase-shift operators that govern primary wave propagation in the anisotropic replacement medium with anelastic losses, based on the derived dispersion relation, and then designing short explicit extrapolation operators in the space–frequency domain based on these phase-shift operators, we can perform wavefield depth extrapolation which takes short-period internal multiples into account in inhomogeneous media. Thus, a table-driven 'true-amplitude' migration scheme is developed, which can approximately eliminate the dispersion effects of the fine-layering together with the geometrical spreading effects in imaging the subsurface based on an extended macro model. Here the quotation marks mean that we assume that the intrinsic absorption has been eliminated separately, e.g. by a time-variant deconvolution process, and 'table-driven' indicates that the depth extrapolation process is performed by selecting the space-variant explicit operators from a pre-calculated operator table (Blacquiere *et al.* 1989). Several authors (Wapenaar & Hermann 1993; Widmaier *et al.* 1996) have proposed to include fine-layering effects into migration. The extended macro model we use is closely related to the conventional macro model used for current migration schemes, except that two stochastic parameters on the rock formations need to be added. The stochastic parameters are derived based on the observation of power-law behaviour of subsurface heterogeneity (Walden & Hosken 1985; Stefani & De 2001), which can be estimated from well logs, from VSP data, or directly from the reflection measurements based on the proposed imaging scheme. It has been observed from well logs that one of the stochastic parameters, the value of the power, does not vary much for different basin types (Stefani & De 2001).

In the proposed migration scheme, the instability, due to boosting amplitudes in the inverse depth extrapolation of a wavefield, is avoided through suppressing the amplitudes of the spatial Fourier transform of the explicit operators for high angles of propagation in the design of the operators. The asymmetric short explicit extrapolation operators, which can boost and decay the amplitudes of wavefields during inverse and forward extrapolations, are designed by adapting the weighted least-squares method (Thorbecke & Rietveld 1994; Zhang *et al.* 2001). The short spatial extent of the derived explicit operators makes it more reasonable for the proposed scheme to handle laterally inhomogeneous media. Of course, the scheme has a dip-angle restriction.

The set-up of this paper is as follows: first oblique wave propagation through 1-D finely layered acoustic media is briefly reviewed; then we present an extended macro model described by a dispersion relation based on average velocities and stochastic parameters; next, the forward and inverse phase-shift operators and the design of spatial explicit operators are discussed; after this an AVA pre-stack migration scheme is proposed; finally, a number of numerical examples are given to illustrate the algorithms.

Transmission response of a layered medium

According to the O'Doherty & Anstey formula, the transmission response of a normal incident wave propagating through a finely layered medium can be described in terms of wavefield extrapolation operators as

$$\tilde{W}_{\mathrm{g}}^{+}(z_m, z_0, \theta = 0, \omega) = \tilde{W}_{\mathrm{p}}^{+}(z_m, z_0, \theta = 0, \omega)\tilde{C}(z_m, z_0, \theta = 0, \omega), \tag{1}$$

where $\tilde{W}_{\mathrm{p}}^{+}(z_m, z_0, \theta = 0, \omega)$ is the extrapolation operator for the primary wave and $\tilde{C}(z_m, z_0, \theta = 0, \omega)$ is a correction operator that accounts for the fine-layering scattering. We call $\tilde{W}_{\mathrm{g}}^{+}(z_m, z_0, \theta = 0, \omega)$ the generalized primary extrapolation operator. The correction operator $\tilde{C}(z_m, z_0, \theta = 0, \omega)$reads

$$\begin{aligned}\tilde{C}(z_m, z_0, \theta = 0, \omega) &= \exp(-A(\omega)\Delta T) \\ &= \exp\left[-\frac{1}{2}R(\omega)\Delta T - j\frac{1}{2}I(\omega)\Delta T\right],\end{aligned} \tag{2}$$

where ΔT is the time of the primary pulse travelling from z_0 to z_m, $R(\omega)$ is the power-spectrum of the reflection coefficients as a function of two-way traveltime (Banik *et al.* 1985), and from the Kramers–Kronig relation $I(\omega)$ should be the Hilbert transform of $R(\omega)$ (Aki & Richards 1980). The functions $R(\omega)$ and $I(\omega)$ define the apparent attenuation and time delay of the transmission response due to the fine-layering scattering, respectively. It has been observed from well logs that in many situations the statistics of the fine-layering are described by fractal Brownian motion (Walden & Hosken 1985). Consequently, $R(\omega)$ in eq. (2) may be expressed as

$$R(\omega) = \upsilon|\omega|^{\alpha}, \tag{3}$$

and its Hilbert transform, $I(\omega)$, is given by

$$I(\omega) = \upsilon \tan(\alpha\pi/2)\mathrm{sign}(\omega)|\omega|^{\alpha}. \tag{4}$$

The analysis of well logs from different basins shows that the value of the power, α, varies from about 0.5 to 0.9 (Stefani & De 2001). The value of υ is determined by the variations of the velocities in the finely layered medium. α and υ can be estimated from sonic logs or from VSP data based on the attenuation and time delay of the pulse (e.g. Walden & Hosken 1985).

Various authors (Burridge & Chang 1989; Shapiro & Zien 1993; Wapenaar *et al.* 1994) extended eq. (1) for oblique wave propagation through a 1-D acoustic medium. For a plane wave with an incident angle of θ, the primary extrapolation operator is given by

$$\tilde{W}_{\mathrm{p}}^{+}(z_m, z_0, \theta, \omega) = \exp(-j\omega\cos\phi\Delta z/c_0), \tag{5}$$

where $\Delta z = z_m - z_0$. We assume a Goupillaud medium (one in which the vertical traveltime across every layer is the same) in our discussion since the stochastic wave theorem is only proven for Goupillaud layered media (Burridge & Chang 1989). Thus, c_0 in eq. (5) denotes the average velocity of the finely layered medium ($c_0 = \sum_{i=1}^{m} c_i/m$) and ϕ is defined as

$$\cos\phi = \sqrt{1 - \left(c_s^2/c_1^2\right)(\sin\theta)^2}, \tag{6}$$

where $c_s^2 = \sum_{i=1}^{m} c_i^2/m$, and c_1 denotes the velocity of the first layer medium. For the fractal Brownian motion model (i.e. eqs 3 and 4), the correction operator may be expressed as (Wapenaar *et al.* 1994)

$$\tilde{C}(z_m, z_0, \theta, \omega) = \exp\left[-A(\omega)(\cos\phi)^{\alpha-n}\Delta z/c_0\right], \tag{7}$$

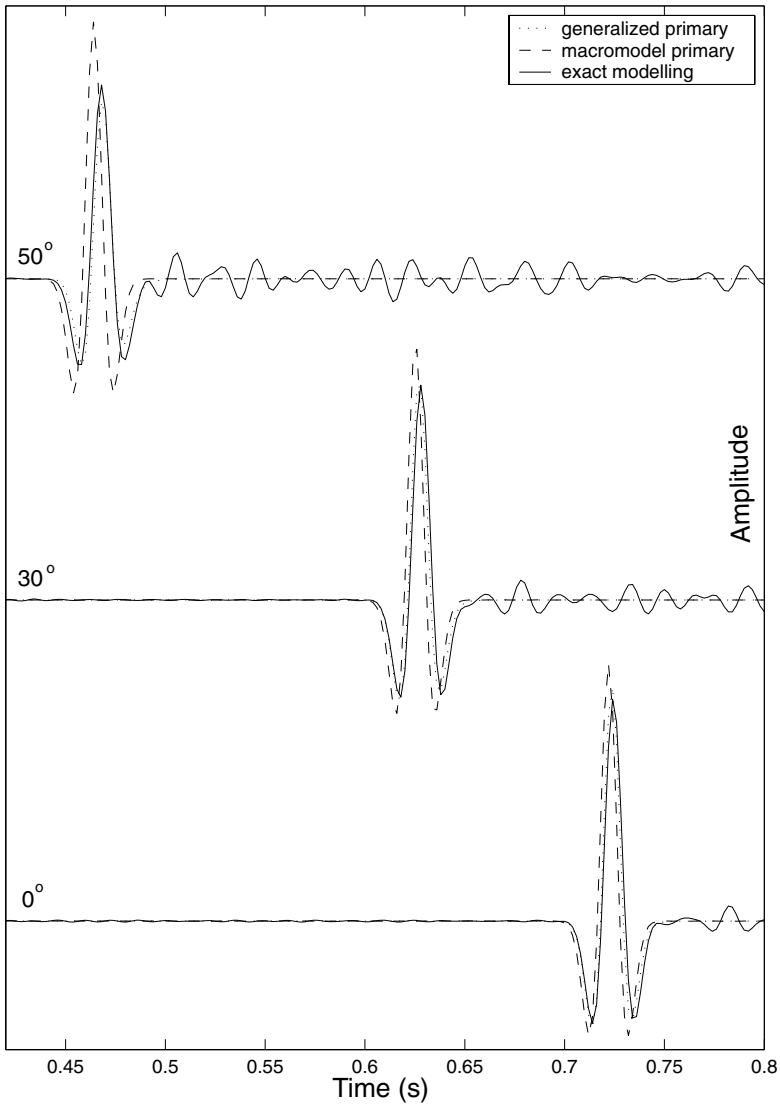

Figure 1. Transmission responses for plane waves with incident angles of 0°, 30° and 50°. The solid-line denotes the exact transmission responses based on the numerical modelling in the true layered medium. The dashed line denotes primary responses based on the average velocity (i.e. macro model). The dotted line denotes the generalized primaries that take the fine-layering scattering into account.

where $n = 4$ when the layered medium contains velocity contrasts only, and $n = 0$ for density contrasts only.

For plane waves with incident angles of 0°, 30° and 50°, Fig. 1 illustrates the comparisons of the primaries, which are generated based on the macro model (i.e. based on eq. 5 and $\phi = \theta$), the generalized primaries, which are obtained based on eqs (5)–(7) that take the fine-layering scattering into account, and exact transmission responses, which are derived from a numerical modelling of the acoustic wave equation in the true layered medium. The synthetic velocity well log for the 1-D layered medium is shown in Fig. 2, and the corresponding α and υ are estimated from the synthetic well log as 0.8779 and 0.0018. The average velocity is 2077 m s^{-1}. From Fig. 1 we can see the significant attenuation and time delay with respect to the primaries due to the fine-layering scattering. Also we find that the generalized primaries match the exact transmission responses well. This shows that the average velocities and the stochastic parameters account for the apparent propagation properties of the finely layered medium.

Extended macro model

The extended macro model aims to replace a finely layered medium by a (piecewise) homogeneous anisotropic medium with anelastic losses in such a way that the primary transmission response of this replacement medium is effectively the same as that of the original finely layered medium. Wapenaar *et al.* (1994) proposed an extended macro model that is described using frequency-dependent vertical and horizontal complex phase velocities. As a result of only matching the coefficients of zeroth-order and second-order ray parameters in the Taylor series expansion, the proposed model has a high angle limitation for the transmission response of the replacement medium to mimic the generalized primary. As an alternative, we directly

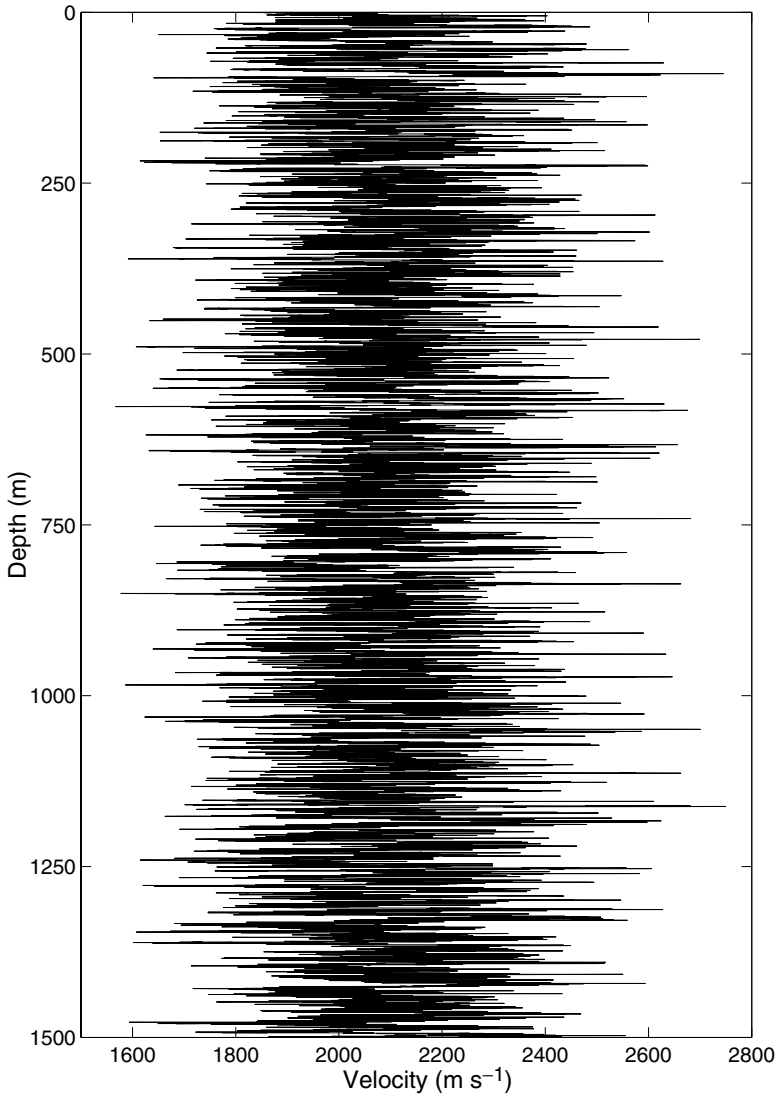

Figure 2. A synthetic velocity well log for an average velocity of 2077 m s^{-1}. The corresponding stochastic parameters are $\alpha = 0.8779$ and $\upsilon = 0.0018$.

derive the dispersion relation for the replacement medium based on the generalized primary, and then define the average velocities and stochastic parameters, that determine the dispersion relation, as a parametrized extended macro model. Thus the proposed method also satisfies the Kramers–Kronig relations for all propagation angles.

For a plane wave with an incident angle of θ, the corresponding horizontal wavenumber reads $k_x = (\omega/c_1)\sin\theta$. From its transmission response as expressed with eqs (5) and (7), we can derive a related complex vertical wavenumber as

$$k_z = [\omega\cos\phi + 0.5I(\omega)(\cos\phi)^{\alpha-n}]/c_0 - j0.5R(\omega)(\cos\phi)^{\alpha-n}/c_0, \tag{8}$$

with

$$\cos\phi = \sqrt{1 - c_s^2 k_x^2/\omega^2}. \tag{9}$$

For a given k_x value we can solve k_z from eqs (8) and (9). This defines a dispersion relation for the replacement medium.

For a finely layered structure that makes an angle of β with the horizontal direction, the corresponding dispersion relation can be obtained as

$$k_z = \frac{\cos\theta}{\cos(\theta-\beta)}[\omega\cos\phi + 0.5I(\omega)(\cos\phi)^{\alpha-n}]/c_0 - j\frac{\cos\theta}{\cos(\theta-\beta)}0.5R(\omega)(\cos\phi)^{\alpha-n}/c_0, \tag{10}$$

with

$$\cos\phi = \sqrt{1 - \frac{c_s^2}{\omega^2}\left[k_x^2\cos 2\beta + \frac{\omega^2}{c_1^2}\sin^2\beta - k_x\left(\omega^2/c_1^2 - k_x^2\right)^{1/2}\sin 2\beta\right]}. \tag{11}$$

Now an extra parameter c_1 appears, which is the velocity of the first layer. Normally it can be approximately replaced using the average velocity of c_0. Moreover, the c_s, the root-mean-square velocity, can also be replaced by c_0. Thus the three parameters, i.e. the average velocity c_0 and the stochastic parameters α and υ (together with the dip-angle of the fine-layering structure), provide a parametrized extended macro model, which is closely related to the conventional

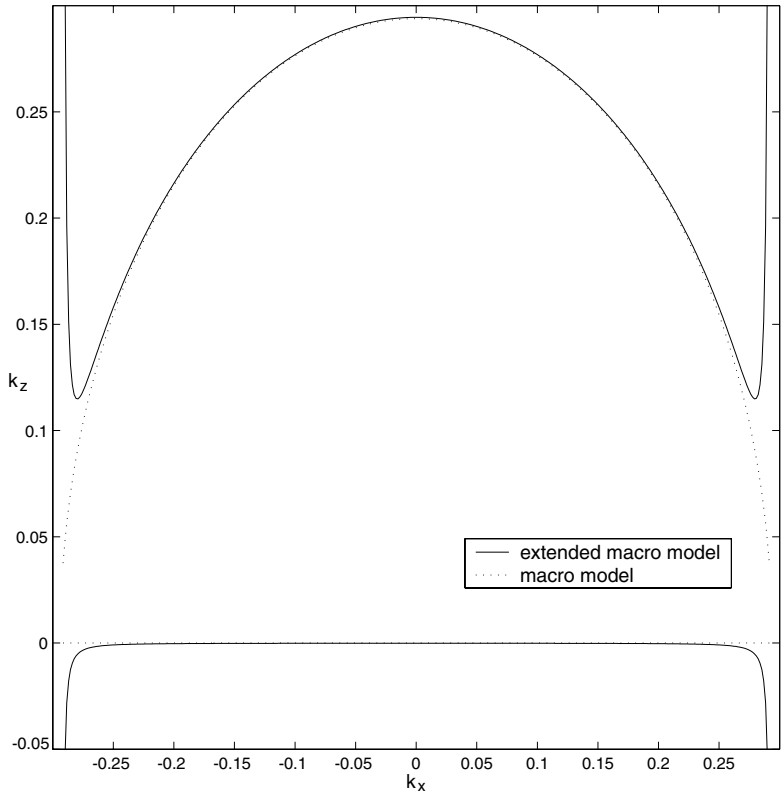

Figure 3. Dispersion relation of the horizontal finely layered medium with its velocity well log as shown in Fig. 2. The positive values (top) are related to the real part of the vertical wavenumber and the negative values (bottom) are related to its imaginary part. The dotted lines denote the conventional dispersion relation with its velocity equal to the corresponding average velocity. The corresponding frequency is $\omega/2\pi = 95$ Hz and the average velocity is $c_0 = 2077$ m s^{-1}.

macro model used for current migration schemes, except that two stochastic parameters on the rock formations have been added.

Fig. 3 illustrates the dispersion relation of the horizontal finely layered medium with its velocity well log as shown in Fig. 2. Fig. 4 further shows the dispersion relation of a tilted structure when the layers have an angle of 15° with the horizontal direction, with its velocity distribution the same as Fig. 2. The frequency is $\omega/2\pi = 95$ Hz and the average velocity is $c_0 = 2077$m s^{-1} for both figures. From Fig. 4 we can find that the replacement medium for a tilted finely layered structure is that of an asymmetrical anisotropic anelastic medium.

Phase-shift operator

From the dispersion relation we can obtain a phase-shift extrapolation operator that can efficiently perform wavefield depth extrapolation and imaging in a laterally invariant medium. The forward phase-shift extrapolation operator for downgoing waves for $\omega > 0$ reads as

$$\tilde{W}_{\mathrm{g}}^{+}(z_{i+1}, z_i, k_x, \omega, c_0, \upsilon, \alpha, \beta) = \exp(-jk_z\Delta z), \quad \Delta z = z_{i+1} - z_i, \tag{12}$$

and the inverse phase-shift extrapolation (downward continuation) operator for upgoing waves can be expressed as

$$\tilde{F}_{\mathrm{g}}^{-}(z_{i+1}, z_i, k_x, \omega, c_0, \upsilon, \alpha, \beta) = \left\{\exp\left[-j\left(k_z^{-}\right)^{*}\Delta z\right]\right\}^{*}, \tag{13}$$

where the superscript $*$ denotes the complex conjugate, and we have (Zhang *et al.* 2001)

$$k_z^{-} = k_z(-k_x, \omega, c_0, \upsilon, \alpha, \beta). \tag{14}$$

The complex conjugate for k_z^{-} in eq. (13) makes the inverse phase-shift operator able to compensate for the attenuation and dispersion due to the fine-layering scattering. However, the stability due to boosting amplitudes appears to be a crucial problem for the inverse phase-shift operator. Hence, even for laterally invariant media, we cannot directly apply the phase-shift operator of eq. (13) to perform inverse wavefield extrapolation.

The stability can be achieved by modifying the part of k_z^{-} associated with high angles, that is, we set the imaginary part of k_z^{-} positive for incident angles exceeding a given value. Hence, beyond this angle the amplitudes are suppressed (of course below this angle the amplitudes remain slightly larger than unity in order to compensate for the scattering losses). In this way, we find a conditional stable operator for a finite number of depth extrapolation steps. This is illustrated by the comparison of the wavenumber spectrum of the inverse phase-shift operator with the derived explicit extrapolation operator in Figs 5 and 6 in the next section.

Explicit extrapolation operator

The phase-shift extrapolation operators are only valid for laterally homogeneous media. However, we have to handle laterally varying media for imaging complex subsurface structures. The explicit extrapolation operator scheme provides an approximation to determine

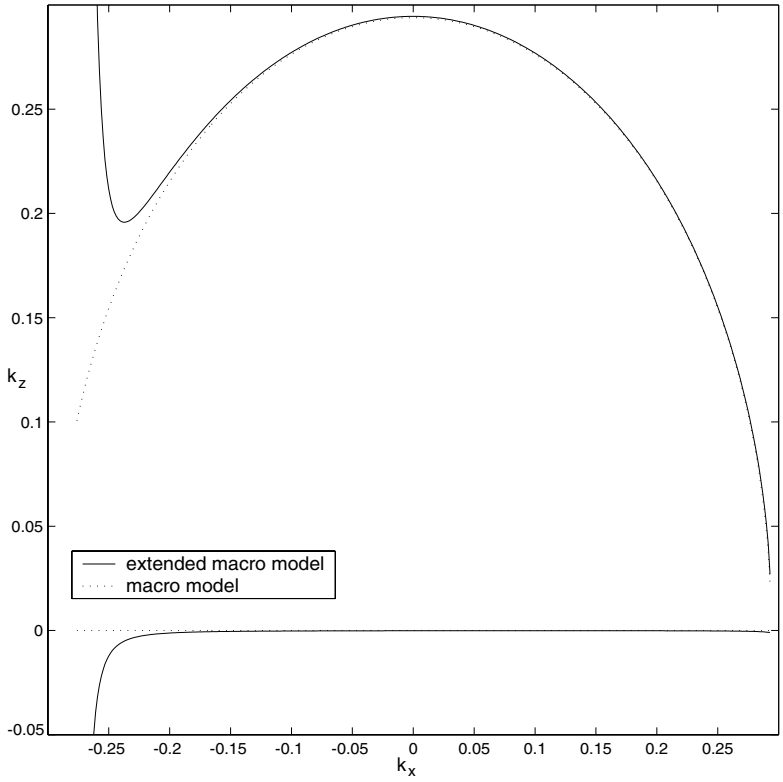

Figure 4. Dispersion relation of the dipping finely layered structure. The finely layered structure is the same as was used for Fig. 3, except that the structure now makes an angle of 15° with the horizontal direction.

the spatial forward and inverse extrapolation operators in a laterally varying medium. The assumption is made that the extended macro model is homogeneous within the spatial extent of the operator. If we obtain a short spatial operator that accurately approximates the phase-shift operator in the wavenumber domain, we can use this short operator to perform the wavefield depth extrapolation in the space domain. It is impossible for a spatial short operator to mimic the phase-shift operator for all wave propagation properties. However, matching the phase-shift operator accurately in a finite range of angles of propagation will be enough for the purpose of eliminating the propagation effects in seismic imaging for a restricted dip range (the operator also needs to decay the energy of the wavefield outside the given range of angles of propagation). This proposes a rule to design the spatial short operator. That is to find a short operator in the space–frequency domain such that its spatial Fourier transform matches the phase-shift operator in the required range of angles of propagation as accurately as possible and its amplitudes decay outside this propagation region. As a result of the fact that the algorithm is implemented by recursive spatial convolution, the short spatial length of the operator will also reduce much computational cost. The explicit extrapolation operator scheme has proven its effectiveness for wavefield extrapolation in inhomogeneous isotropic and anisotropic macro models (e.g. Holberg 1988; Zhang *et al.* 2001).

For the explicit extrapolation operator scheme, the task to stabilize the inverse extrapolation operators by suppressing the wavefield with a high angle of propagation can be easily accomplished through taking the requirement of stability into account when determining the maximum angle of propagation.

There exist a number of available methods for designing symmetric short operators (e.g. Holberg 1988; Hale 1991). However, an asymmetric short operator needs to be designed here. In contrast to Holberg's non-linear least-squares and Hale's Taylor series expansion methods, the weighted least-squares method (Thorbecke & Rietveld 1994) can derive a stable, highly accurate short operator with a very low computational cost in an isotropic lossless medium. The method has been extended to design asymmetric short operators by Zhang *et al.* (2001). Here we further adapt the weighted least-squares method to design short operators for an anisotropic lossy medium.

With a complex vector $\mathbf{Y}_1 + j\mathbf{Y}_2$ denoting the desired short operator, the discretized values of its spatial Fourier transform can be expressed with a complex vector as $\tilde{\mathbf{Y}} = (\mathbf{\Gamma}_1\mathbf{Y}_1 - \mathbf{\Gamma}_2\mathbf{Y}_2) + j(\mathbf{\Gamma}_1\mathbf{Y}_2 + \mathbf{\Gamma}_2\mathbf{Y}_1)$. Here the elements of the matrices $\mathbf{\Gamma}_1$ and $\mathbf{\Gamma}_2$ are, respectively, defined as $\cos(m\Delta k_x n\Delta x)$ and $\sin(m\Delta k_x n\Delta x)$ for $m = -M, M$; $n = -N, N$, where $(2N + 1)\Delta x$ is the spatial length of the short operator and $\Delta k_x = 1/(2\Delta x M)$ is the horizontal wavenumber interval. Defining the sum-of-squares error as

$$e = \left(\mathbf{Y}_1^{\mathrm{T}}\mathbf{\Gamma}_1^{\mathrm{T}} - \mathbf{Y}_2^{\mathrm{T}}\mathbf{\Gamma}_2^{\mathrm{T}} - \tilde{\mathbf{Y}}_{er}^{\mathrm{T}}\right)\mathbf{\Lambda}(\mathbf{\Gamma}_1\mathbf{Y}_1 - \mathbf{\Gamma}_2\mathbf{Y}_2 - \tilde{\mathbf{Y}}_{er}) + \left(\mathbf{Y}_2^{\mathrm{T}}\mathbf{\Gamma}_1^{\mathrm{T}} + \mathbf{Y}_1^{\mathrm{T}}\mathbf{\Gamma}_2^{\mathrm{T}} - \tilde{\mathbf{Y}}_{ei}^{\mathrm{T}}\right)\mathbf{\Lambda}(\mathbf{\Gamma}_1\mathbf{Y}_2 + \mathbf{\Gamma}_2\mathbf{Y}_1 - \tilde{\mathbf{Y}}_{ei}), \quad (15)$$

we can transform the design of the short operator into an unconstrained optimization problem, i.e. minimizing e. Here the complex vector $\tilde{\mathbf{Y}}_e = \tilde{\mathbf{Y}}_{er} + j\tilde{\mathbf{Y}}_{ei}$ contains the discretized values of the

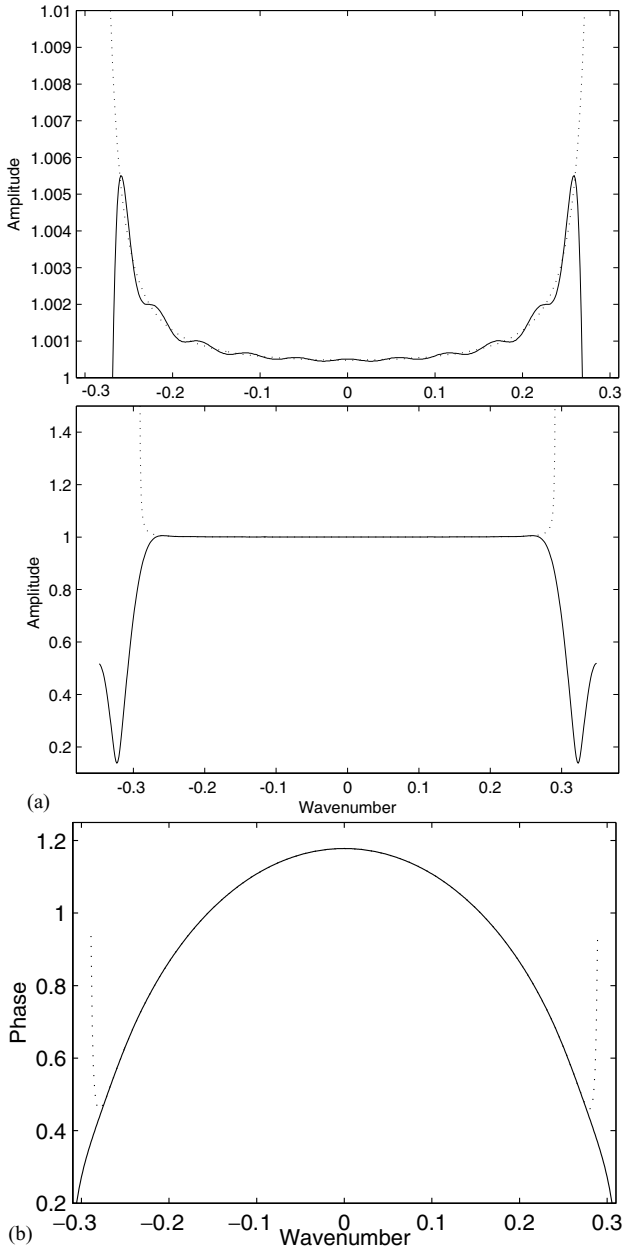

Figure 5. (a) Amplitude spectrum for a stabilized symmetric 25-point explicit operator for inverse wavefield extrapolation (solid lines). The dotted lines are related to the amplitude spectrum of the exact inverse phase-shift operator. The top shows a detailed view around 1.005. Note the stabilization effects of the proposed scheme: the high amplitudes are suppressed. (b) Phase spectrum for a stabilized symmetric 25-point explicit operator for inverse wavefield extrapolation (solid line). The dotted line is related to the phase spectrum of the exact inverse phase-shift operator.

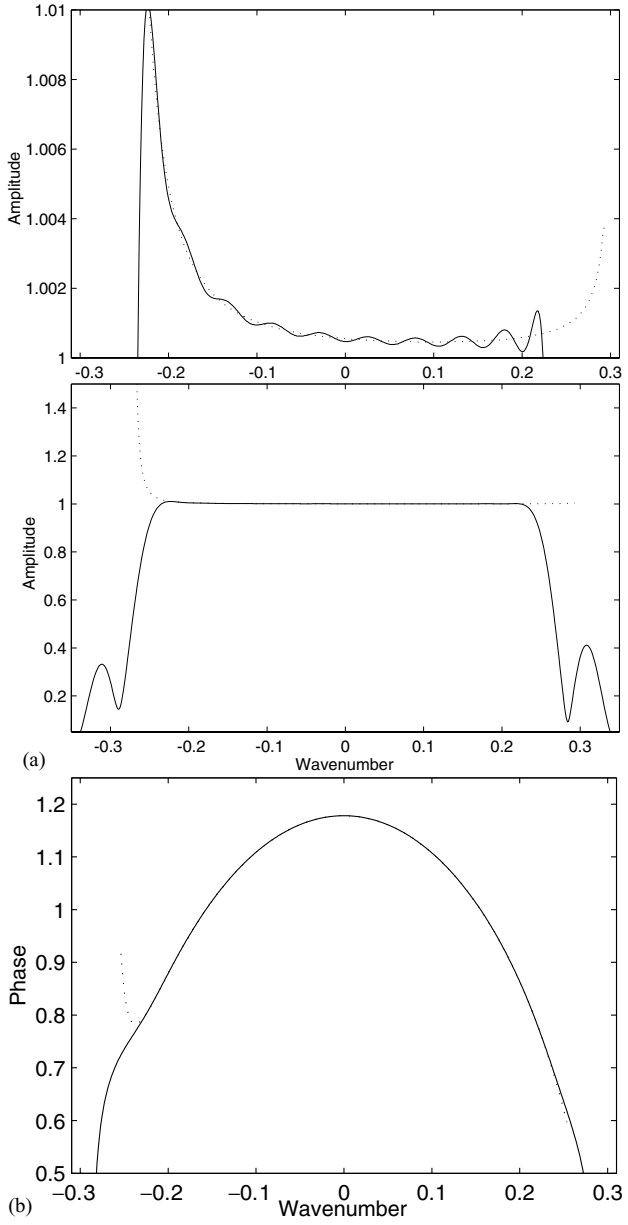

Figure 6. (a) Amplitude spectrum for a stabilized asymmetric 25-point explicit operator (solid lines). The dotted lines are related to the amplitude spectrum of the exact inverse phase-shift operator. The top shows a detailed view around 1.005. Everything is the same as in Fig. 5(a), except that the corresponding finely layered structure makes an angle of 15° with the horizontal direction. (b) Phase spectrum for a stabilized asymmetric 25-point explicit operator (solid line). The dotted line is related to the phase spectrum of the exact inverse phase-shift operator. Everything is the same as in Fig. 5(b), except that the corresponding finely layered structure makes an angle of 15° with the horizontal direction.

phase-shift operator for $|m\Delta k_x| \leq (\omega/c_0)\ \sin(\theta_{\max})$, and for $|m\Delta k_x| > (\omega/c_0)\sin(\theta_{\max})$ the components of $\tilde{\mathbf{Y}}_e$ are given by

$$\mathrm{Re}(y_m) = \mathrm{Re}(y_c)\exp\left\{-\gamma_1\left[|m\Delta k_x| - (\omega/c_0)\sin(\theta_{\max})\right]^2\right\}, \quad (16a)$$

$$\mathrm{Im}(y_m) = \mathrm{Im}(y_c)\exp\left\{-\gamma_2\left[|m\Delta k_x| - (\omega/c_0)\sin(\theta_{\max})\right]^2\right\}, \quad |m\Delta k_x| < \omega/c_0, \quad (16b)$$

$$\mathrm{Im}(y_m) = 0, \qquad |m\Delta k_x| \geq \omega/c_0, \quad (16c)$$

where y_c is the value of the phase-shift operator for $k_x = (\omega/c_0)\sin(\theta_{\max})$, y_m is the component of $\tilde{\mathbf{Y}}_e$ that corresponds to $k_x = m\Delta k_x$, $\theta_{\max}$ is determined according to the spatial sampling interval and the accepted maximum magnitude for extrapolating a finite number of steps (the more steps, the smaller $\theta_{\max}$), and γ_1 and γ_2 are parameters selected according to the decay requirement for the

amplitudes. The weight matrix $\mathbf{\Lambda}$ in eq. (15) is a real-valued diagonal matrix, the elements of which are 1.0 for $|m\Delta k_x| \leq (\omega/c_0)\sin(\theta_{\max})$ and a very small value (e.g. 10^{-5}) for $|m\Delta k_x| > (\omega/c_0)\sin(\theta_{\max})$. From the optimization problem of eq. (15) we can solve the short operator as

$$\begin{Bmatrix} \mathbf{Y}_1 \\ \mathbf{Y}_2 \end{Bmatrix} = \begin{bmatrix} \mathbf{\Gamma}_1^{\mathrm{T}}\mathbf{\Lambda}\mathbf{\Gamma}_1 + \mathbf{\Gamma}_2^{\mathrm{T}}\mathbf{\Lambda}\mathbf{\Gamma}_2 & \mathbf{\Gamma}_2^{\mathrm{T}}\mathbf{\Lambda}\mathbf{\Gamma}_1 - \mathbf{\Gamma}_1^{\mathrm{T}}\mathbf{\Lambda}\mathbf{\Gamma}_2 \\ \mathbf{\Gamma}_1^{\mathrm{T}}\mathbf{\Lambda}\mathbf{\Gamma}_2 - \mathbf{\Gamma}_2^{\mathrm{T}}\mathbf{\Lambda}\mathbf{\Gamma}_1 & \mathbf{\Gamma}_1^{\mathrm{T}}\mathbf{\Lambda}\mathbf{\Gamma}_1 + \mathbf{\Gamma}_2^{\mathrm{T}}\mathbf{\Lambda}\mathbf{\Gamma}_2 \end{bmatrix}^{-1} \times \begin{Bmatrix} \mathbf{\Gamma}_1^{\mathrm{T}}\mathbf{\Lambda}\tilde{\mathbf{Y}}_{er} + \mathbf{\Gamma}_2^{\mathrm{T}}\mathbf{\Lambda}\tilde{\mathbf{Y}}_{ei} \\ \mathbf{\Gamma}_1^{\mathrm{T}}\mathbf{\Lambda}\tilde{\mathbf{Y}}_{ei} - \mathbf{\Gamma}_2^{\mathrm{T}}\mathbf{\Lambda}\tilde{\mathbf{Y}}_{er} \end{Bmatrix}. \quad (17)$$

Fig. 5(a) shows an amplitude spectrum in the wavenumber domain for a 25-point ($N = 12$) symmetric explicit inverse operator that corresponds to the dispersion relation of Fig. 3. Here we assume the accepted maximum magnitude is 1.01, for which the maximum angle of propagation is 60°. Fig. 5(b) further illustrates the phase spectrum of this 25-point operator. Fig. 6(a) shows an amplitude spectrum in the wavenumber domain for a 25-point ($N = 12$) asymmetric explicit inverse operator that corresponds to the dispersion relation of Fig. 4 when the layers have an angle of 15° with the horizontal direction. The corresponding phase spectrum of this operator is illustrated in Fig. 6(b). The parameters for both Figs 5 and 6 are $\Delta x = 9$ m, $\Delta z = 4$ m, $\omega/2\pi = 95$ Hz, $c_0 = 2077$ m s^{-1}. For Fig. 6 we assume the accepted maximum magnitude is 1.018, for which the maximum angle of propagation is 50°. From Figs 5 and 6 we find that the derived explicit inverse operators match the original operators well below the maximum angle of propagation. The comparisons of the amplitude spectra of the phase-shift operators with the derived short operators illustrate the stabilizing effects of the proposed scheme. It should be noted that the fact that the maximum magnitudes of the derived short operator does not approach the accepted maximum magnitudes in Figs 5(a) and 6(a) is due to the fact that the frequency corresponding to the operators is $0.8\omega_{\max}$ instead of $\omega_{\max}$.

The scheme is implemented by pre-calculating an operator table and then selecting the space-variant operator at each gridpoint

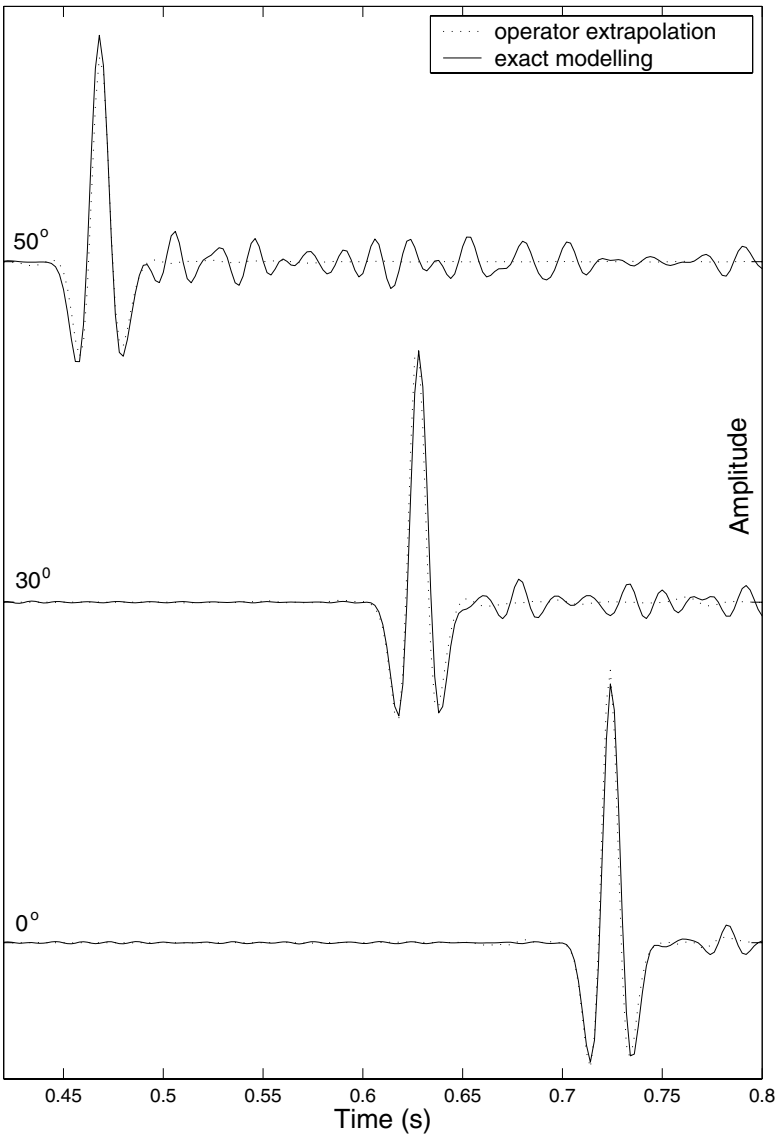

Figure 7. Comparisons of the transmission responses of the explicit depth extrapolation with that of exact numerical modelling in the true finely layered medium. The plane waves have incident angles of 0°, 30° and 50°.

according to the local macro velocity and the two stochastic parameters during the depth extrapolation process.

AVA migration

The major factors affecting the amplitudes in seismic data may be outlined as: geometrical spreading, interface reflection coefficients, intrinsic absorption, short-period internal multiples and transmission losses. Conventional pre-stack migration schemes only compensate for the geometrical spreading, so the image does not represent the true reflectivity of the subsurface. The angle-independent intrinsic absorption can be treated in a pre-processing step by so-called inverse Q-filters or in the migration process itself (Mittet *et al.* 1995; Zhang & Wapenaar 2002). Short-period internal multiples due to high discontinuities of rock formations, deserve attention for imaging the true reflectivity of the subsurface with better resolution. In the foregoing sections, we developed an explicit extrapolation operator scheme that can compensate for the angle-dependent dispersion and amplitude losses due to fine-layering scattering (i.e. short-period internal multiples). Based on this algorithm, we now propose an AVA pre-stack migration scheme.

The true-reflectivity imaging can be achieved using two alternative ways. One is given by

$$\Phi(x,z)=\int \frac{P^{\mathrm{U}}(x,z,\omega)\{P^{\mathrm{D}}(x,z,\omega)\}^{*}}{P^{\mathrm{D}}(x,z,\omega)\{P^{\mathrm{D}}(x,z,\omega)\}^{*}+\varepsilon}\,d\omega, \tag{18}$$

where $P^{\mathrm{D}}(x,z,\omega)$ is the one-way downgoing wavefield obtained by recursive convolutions with the forward explicit extrapolation operators, $P^{\mathrm{U}}(x,z,\omega)$ is the one-way upgoing wavefield obtained by recursive convolutions with the inverse explicit extrapolation operators and ε a small stabilization constant. The other imaging condition is developed by designing forward extrapolation operators that also compensate for amplitude losses rather than attenuating wavefields. Fortunately, this forward extrapolation operator can be easily obtained by taking the complex conjugate of the corresponding inverse extrapolation operator. With $[P^{\mathrm{D}}(x,z,\omega)]'$ denoting the one-way forward extrapolated downgoing wavefield that is obtained by recursive convolutions with the derived forward explicit extrapolation operators, the imaging condition can be expressed as

$$\Phi(x,z)=\int P^{\mathrm{U}}(x,z,\omega)\{[P^{\mathrm{D}}(x,z,\omega)]'\}^{*}\,d\omega. \tag{19}$$

The imaging condition of eq. (19) was first proposed by Mittet *et al.* (1995) for imaging anelastic media. In both cases, $\Phi(x,z)$ represents the reflectivity as a function of depth (z) and lateral position (x), which can, for each shot record, be translated to an angle of incidence.

The advantage of the second imaging condition is that only one operator table is needed, which reduces the computational costs. However, from a theoretical point of view the imaging condition of eq. (18) is preferred. Numerical studies on imaging in anelastic media (Zhang & Wapenaar 2002) indeed show that the imaging condition of eq. (18) gives better results than the imaging condition of eq. (19). Therefore, in the remainder of this paper we use the imaging condition of eq. (18).

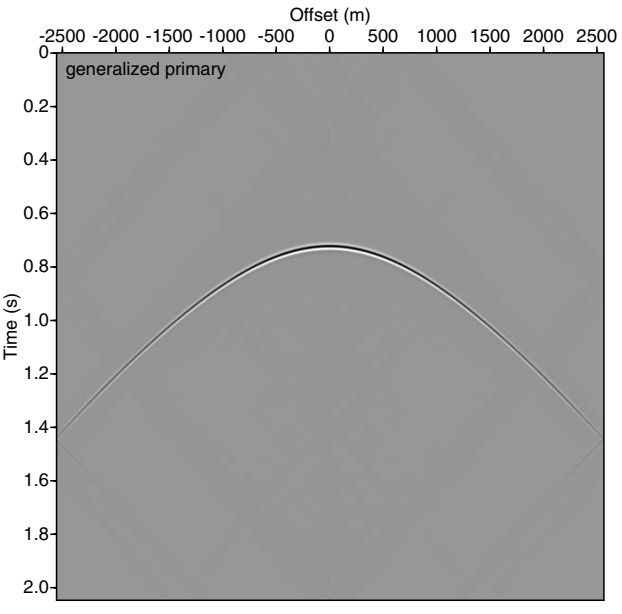

Figure 8. The generalized primary response of a line source for the finely layered medium with its velocity well log as shown in Fig. 2.

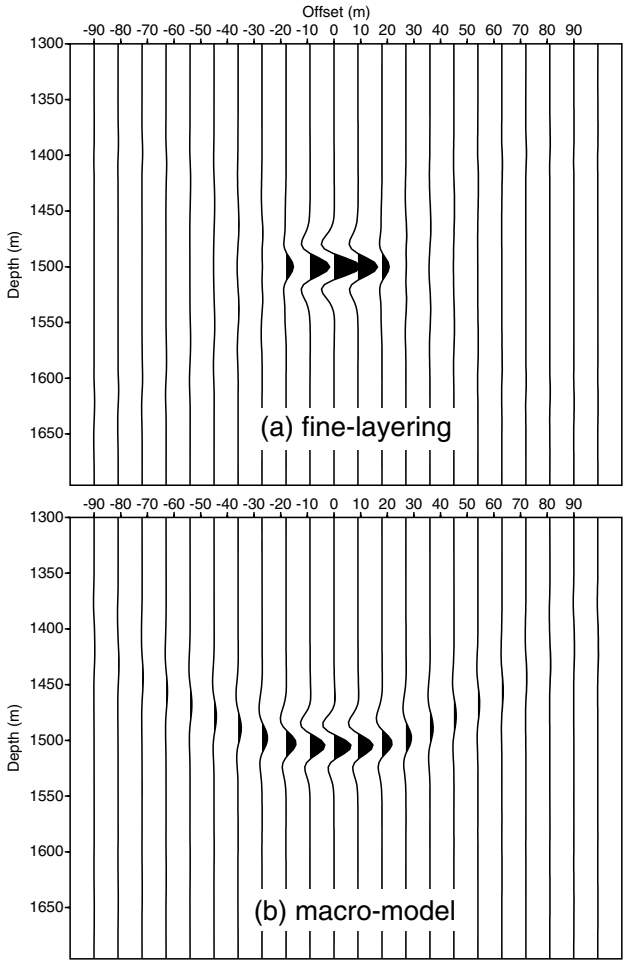

Figure 9. Comparison of the inverse depth extrapolation for taking the fine-layering scattering into account and neglecting it. The result in (a) is obtained using the correct stochastic parameters and average velocity. The result in (b) is obtained only using the average velocity but neglecting the highly discontinuous properties of the velocity distribution. Note the fact that (b) fails to focus at a point. The parameters we use are $\theta_{\max}=60^{\circ}$, $\Delta x=9$ m and $\Delta z=4$ m.

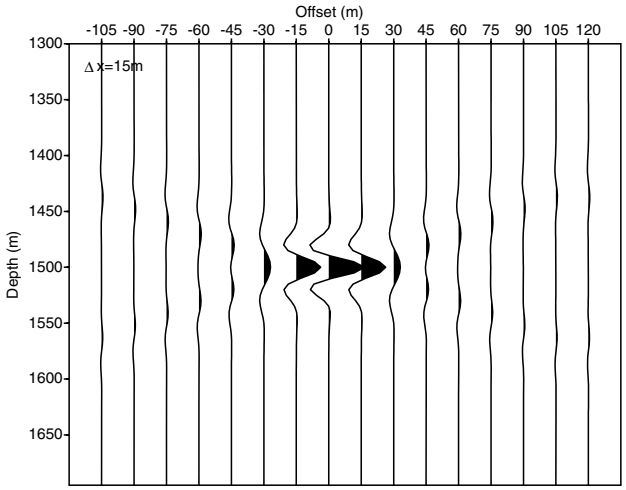

Figure 10. Suppressing the aliasing due to sparse spatial sampling. The result of the inverse depth extrapolation is obtained based on a sparse sampling spacing of 15 m for the line source response of Fig. 8. A 25-point operator with a maximum angle of propagation of 35° is used.

The proposed pre-stack migration scheme can also effectively suppress the aliasing due to sparse spatial sampling by controlling the maximum angle of propagation in the design of the explicit extrapolation operators. This means that we choose $\theta_{\max}$ such that $\sin(\theta_{\max}) \leq \pi c_0/(\omega_{\max}\Delta x)$ besides taking the accepted maximum magnitude into account in determining the maximum angle of propagation. Here $\omega_{\max}$ is the maximum frequency of the seismic data.

NUMERICAL EXAMPLES

Depth extrapolation

The performance of the proposed forward explicit extrapolation operators is illustrated through comparing the extrapolation results with the exact transmission responses of the finely layered medium. The velocity log is as shown in Fig. 2. Fig. 7 illustrates the comparisons for plane waves with incident angles of 0°, 30° and 50°. The result for 'operator extrapolation' is obtained by performing recursively spatial convolutions as in a homogeneous medium, using the derived short operators from $z = 0$ to 1500 m with $\Delta z = 4$ m and $\Delta x = 9$ m. A 25-point short operator with a maximum angle of propagation of 60° is used. From Fig. 7 we see that the generalized primaries of the two methods agree well. The small errors for the amplitudes are of the same order as those of the generalized primaries compared with the exact transmission responses, as shown in Fig. 1, which originated from the stochastic wave theory. The proposed inverse explicit extrapolation operators are illustrated by performing inverse wavefield extrapolation for a generalized primary response of a line source, as shown in Fig. 8. The line source is located at the origin and receivers are positioned at $z = 1500$ m for a medium with its velocity well log as shown in Fig. 2. Fig. 9 illustrates the results of inverse depth extrapolations, using different kinds of explicit operators. One kind of operator is designed using the correct stochastic parameter and average velocity. The corresponding result is shown in Fig. 9(a). The other kind of operators is obtained only using the average velocity (i.e. the macro model) but ignoring the highly discontinuous properties of the velocity distribution. This is shown in Fig. 9(b). By comparing Figs 9(a) and (b) we find that the macromodel result does not focus at one point, which will lead to dispersed images in seismic migration.

A 25-point operator with $\theta_{\max} = 60°$, $\Delta x = 9$ m and $\Delta z = 4$ m is used for Fig. 9. With $c_0 = 2077$ m s^{-1} and $\omega_{\max} = 120$ Hz, the spatial sampling should be 8.6 m for $\theta_{\max} = 90°$. By taking a sparse

Table 1. Stochastic parameters and density.

Layer	1	2	3	4
υ	0.0011	0.0016	0.0010	0.0004
α	0.8286	0.8234	0.8907	0.8243
ρ (kg m^{-3})	1000	1200	1800	2600

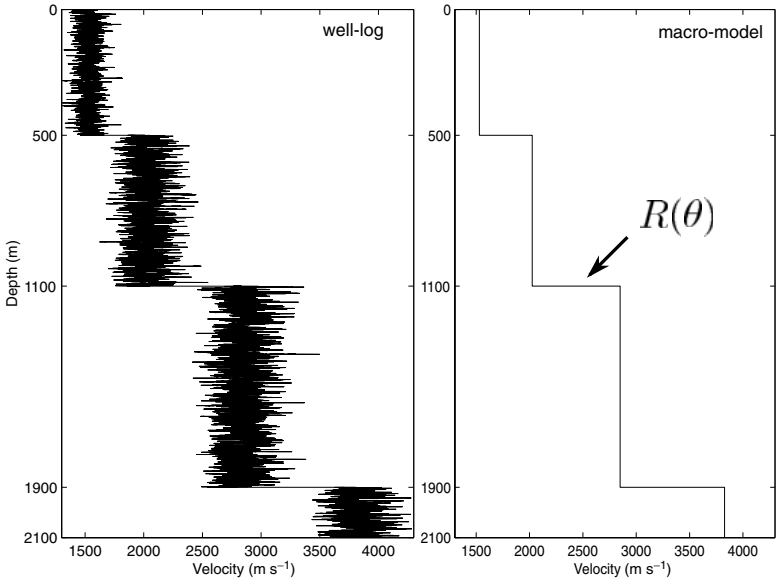

Figure 11. A synthetic velocity well log for a layered medium. The right is the corresponding macro model.

sampling of 15 m for the line source response of Fig. 8, we still obtain a good focusing effect, as illustrated in Fig. 10, by designing the short operators with $\theta_{\max} = 35^\circ$ and $\Delta z = 5$ m. This shows that the proposed scheme can effectively suppress the aliasing due to sparse spatial sampling.

A zero-phase Ricker wavelet with a peak frequency of 40 Hz is used for all examples.

Pre-stack depth migration

A synthetic seismic experiment is designed to test the proposed AVA pre-stack migration scheme. The seismic data set is generated through numerical modelling of the two-way acoustic wave equation in a true finely layered medium using the reflectivity method. The synthetic velocity well log of the layered medium is illustrated in the left of Fig. 11, and the corresponding macro model is shown in the right of Fig. 11. The associated stochastic parameters are listed in Table 1, which together with the macro model in the right of Fig. 11 provide an extended macro model for the highly discontinuous velocity distribution as shown in the left of Fig. 11. The densities corresponding to the macro model are also listed in Table 1. One shot gather is shown in Fig. 12. The source is a zero-phase Ricker wavelet with a peak frequency of 40 Hz. The migrated results for this shot gather with the extended macro model as well as with the standard macro model are illustrated in Figs 13(a) and (b). A 25-point short operator with $\theta_{\max} = 60^\circ$ was used with $\Delta x = 8$ m and $\Delta z = 4$ m. The migration with the standard macro model means that the highly discontinuous properties of the velocity distribution are ignored. From Fig. 13 we see that the main reflectors are imaged clearly. Fig. 14 shows a detailed view of the comparisons of two migrated results for the offsets of 0 and 600 m and the ray angle of 28° in the vicinities of three reflectors. From Fig. 14 we find that the migrated results that take the fine-layering scattering into account are positioned at the correct locations, i.e. 500, 1100 and 1900 m. Also, significant differences of the amplitudes can be seen for the two migrated results. Fig. 15 further shows the comparisons of the offset-dependent reflectivity of the two migrated results with the exact reflection coefficient at the depth level of 1100 m,

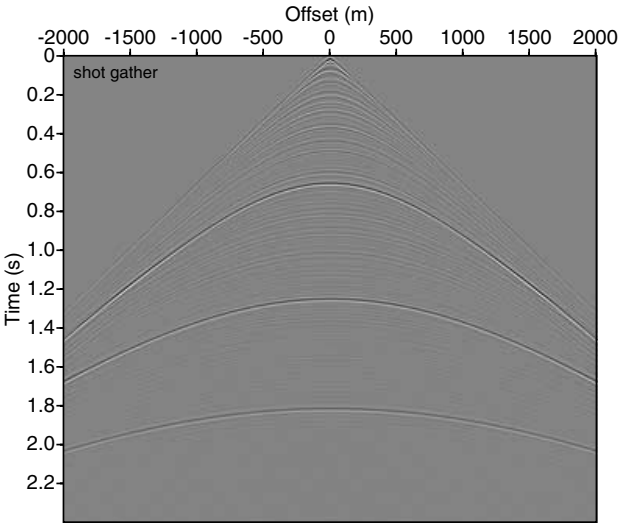

Figure 12. Shot gather for a zero-phase Ricker wavelet with a peak frequency of 40 Hz. The shot gather is obtained using the reflectivity method in the true finely layered medium.

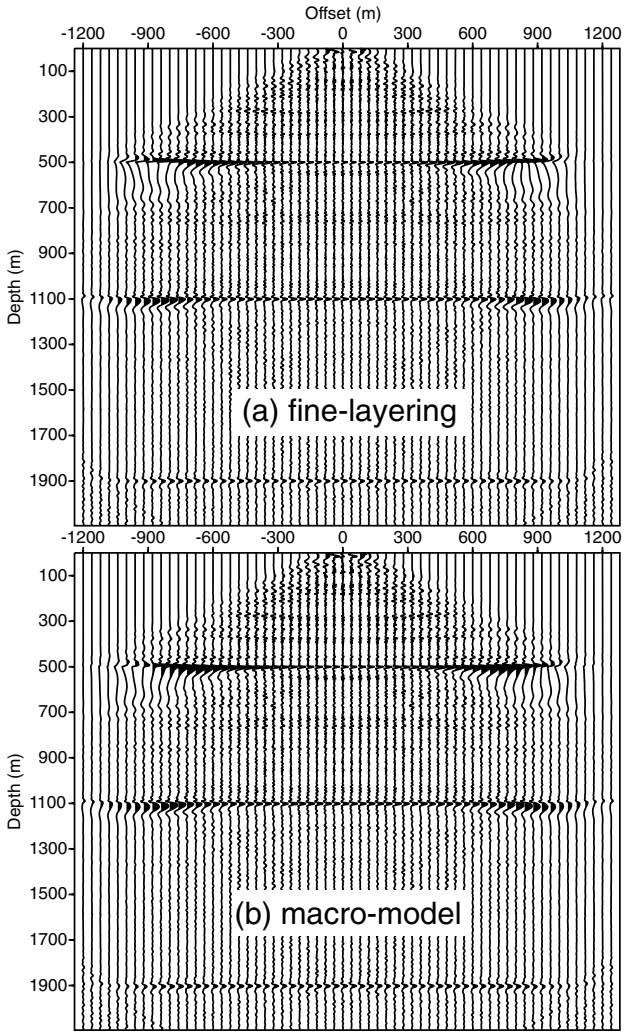

Figure 13. Shot-record migration results. The result in (a) is obtained using an extended macro model that takes the fine-layering scattering into account. The result in (b) is obtained using the macro model that ignores the highly discontinuous properties of the velocity distribution.

as indicated by the arrow in Fig. 11. From this comparison we observe that the migration result, which takes fine-layering scattering into account, better approaches the exact reflection coefficient. The match is, however, not perfect for the following reasons. First, the exact reflection coefficient is based on the velocity and density contrasts at the second boundary of the *macro* model, therefore this 'exact reflection coefficient' is exact for the macro model but it is an approximation for the true finely layered medium. Secondly, the migration result reveals a noisy character due to interference with the reflectors above and below the depth level of 1100 m.

The reason that we use a laterally invariant medium is that the only available modelling tool for the true velocity model, consisting of 21 000 layers as illustrated in Fig. 11, is the reflectivity method. However, the migration algorithm we use is based on the explicit extrapolation operators, that has been proven to be effective for both isotropic and anisotropic laterally varying macro models. Hence, it is reasonable to state that the proposed scheme can efficiently be applied for a practical subsurface that is moderately inhomogeneous at the macro scale and highly discontinuous at the subwavelength scale.

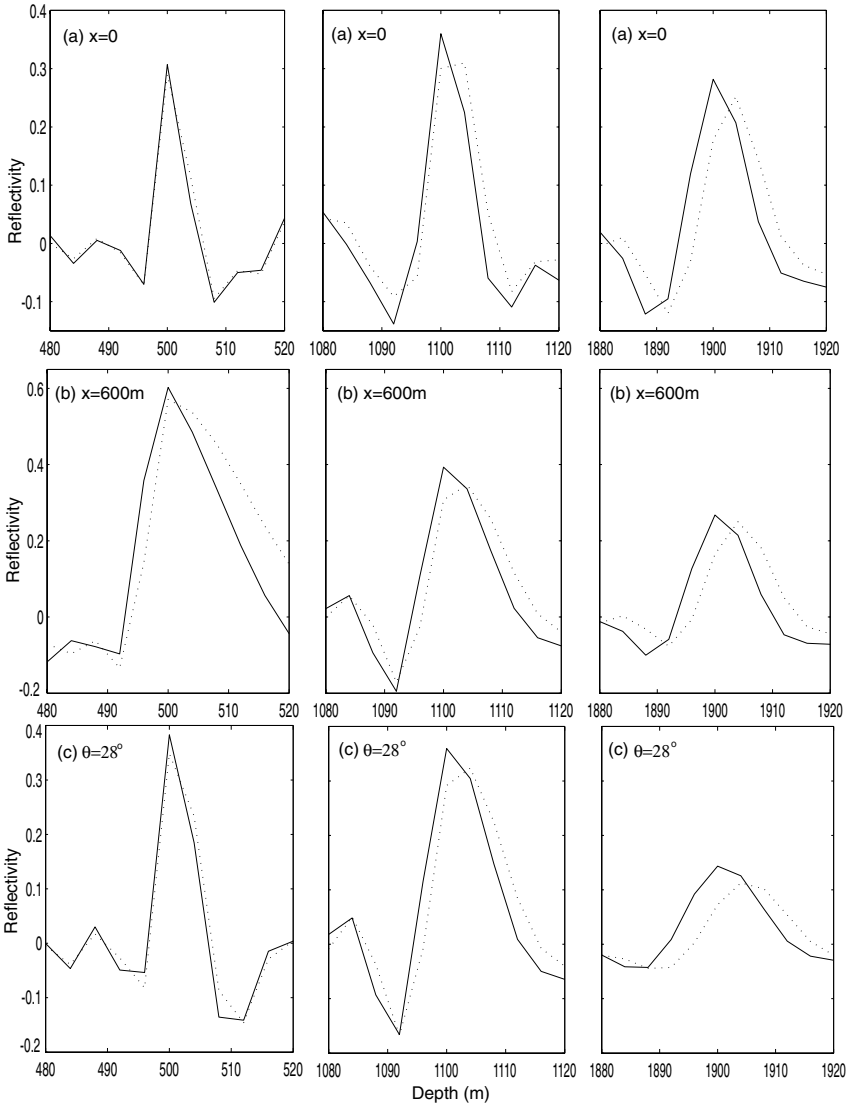

Figure 14. Detailed views of the comparison of the two migration results in Fig. 13. The first two rows are for the offsets of 0 and 600 m, and the last row is for the ray angle of 28°. The columns are related to three main reflectors at 500, 1100 and 1900 m. (Dotted, macro model; solid, extended macro model, including fine layering).

CONCLUSION

A method for wavefield depth extrapolation in a subsurface that is moderately inhomogeneous at the macro scale and highly discontinuous at the subwavelength scale has been presented. Moreover, a pre-stack migration scheme, which can image the true reflectivity of the subsurface by eliminating the geometrical spreading effects as well as the dispersion effects of the finely layering, has been proposed. The statistical behaviour exhibited by the subsurface heterogeneity (fractal Brownian motion) is used to set up a parametrized extended macro model, which can quantify the effects on the transmission response of the short-period internal multiples due to the highly discontinuous properties of the rock formations. The proposed extended macro model introduces an anisotropic anelastic medium to mimic the apparent propagation properties of the highly discontinuous rock formations. Furthermore, a medium with varying macro model can mimic the propagation properties of a true subsurface. In this paper the resulting replacement medium is described by the dispersion relation instead of a real physical state. The phase-shift operators are developed for the replacement medium based on the dispersion relation, and then short spatial explicit extrapolation operators are designed based on the derived phase-shift operators. These are used to perform wavefield depth extrapolation in inhomogeneous replacement media. The weighted least-squares method is adapted to design the symmetric and asymmetric short explicit extrapolation operators, and the stability for inverse wavefield extrapolation is achieved by controlling the maximum angle of propagation of the wavefield in the design of the short operators. Moreover, the aliasing due to sparse spatial sampling can be effectively suppressed in this angle-controlled process. The proposed AVA migration scheme is implemented based on the extended macro model by pre-calculating an operator table and then selecting the space-variant operator during the depth extrapolation process.

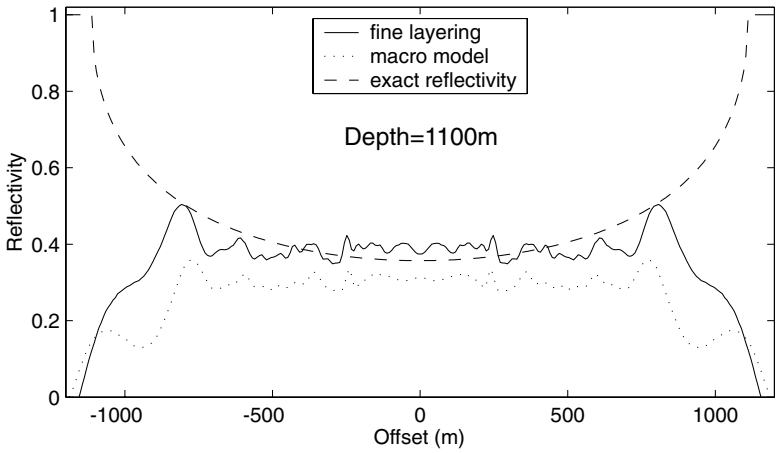

Figure 15. Comparison of the reflectivity of the two migration results with the exact reflection coefficients at the depth level of the second main reflector. The solid line denotes the migration result at the depth level of 1100 m obtained using an extended macro model that takes the fine-layering scattering into account, the dotted line denotes the migration result obtained using the macro model that ignores the highly discontinuous properties of the velocity distribution and the dashed line denotes the exact reflection coefficients based on the velocity and density contrasts at the second boundary of the macro model.

The accuracy of the proposed forward explicit extrapolation operators is demonstrated by comparing the forward extrapolation results with exact transmission responses of the true finely layered medium. The good performance of the derived explicit inverse operators is illustrated by the inverse depth extrapolation of a generalized primary response of a line source that includes angle-dependent dispersion and amplitude losses. A synthetic data set, obtained using the reflectivity method for a finely layered medium, is used to test the proposed AVA migration scheme. The numerical example shows a significant improvement of the obtained angle-dependent reflectivity of the subsurface when taking the fine-layering scattering into account.

ACKNOWLEDGMENTS

The first author (JZ) thanks the Netherlands Research Centre for Integrated Solid Earth Science for supporting his research fellowship at Delft University of Technology. The authors thank Dr D. J. Verschuur of Delft University of Technology for providing us with his reflectivity method code.

REFERENCES

Aki, K. & Richards, P.G., 1980. *Quantitative Seismology,* Freeman, San Francisco

Banik, N.C., Lerche, T. & Shuey, R.T., 1985. Stratigraphic filtering, Part I: Derivation of O'Doherty–Anstey formula, *Geophysics,* **50,** 2768–2774.

Blacquiere, G., Debeye, H.W.J., Wapenaar, C.P.A. & Berkhout, A.J., 1989. 3D table-driven migration, *Geophys. Prospect.,* **37,** 925–958.

Burridge, R. & Chang, H.W., 1989. Multimode, one-dimensional wave propagation in a highly discontinuous medium, *Wave Motion,* **11,** 231–249.

Hale, D., 1991. Stable explicit depth extrapolation of seismic wavefields, *Geophysics,* **56,** 1770–1777.

Hermann, F.J. & Wapenaar, C.P.A., 1992. Macro description of fine layering: proposal for an extended macro model, *62nd Ann. Int. SEG Mtg,* New Orleans, Expanded Abstr., 1263–1266. Society of Exploration Geophysicists, Tulsa, OK, USA.

Holberg, O., 1988. Toward optimum one-way wave propagation, *Geophys. Prospect.,* **36,** 99–114.

Mittet, R., Sollie, R. & Hokstad, K., 1995. Prestack depth migration with compensation for absorption and dispersion, *Geophysics,* **60,** 1485–1494.

O'Doherty, R.F. & Anstey, N.A., 1971. Reflections on amplitudes, *Geophys. Prospect.,* **19,** 430–458.

Schoenberger, M. & Levin, F.K., 1979. The effect of subsurface sampling on one-dimensional synthetic seismograms, *Geophysics,* **44,** 1813–1829.

Shapiro, S.A. & Zien, H., 1993. The O'Doherty–Anstey formula and localization of seismic waves, *Geophysics,* **58,** 736–740.

Stefani, J. & De, G.S., 2001. On the power-law behavior of subsurface heterogeneity, *71st Ann. Int. SEG Mtg,* San Antonio, Expanded Abstract, 2033–2036. Society of Exploration Geophysicists, Tulsa, OK, USA.

Thorbecke, J.T. & Rietveld, W.E.A., 1994. Optimum extrapolation operators: a comparison, *56th Ann. Int. Mtg, Eur. Assoc. Expl. Geophys.,*Exp., Abstracts, P105. European Association of Exploration Geophysicists, Zeist, the Netherlands.

Walden, A.T. & Hosken, J.W.J., 1985. An investigation of the spectral properties of primary reflection coefficients, *Geophys. Prospect.,* **33,** 400–435.

Wapenaar, C.P.A. & Hermann, F.J., 1993. True amplitude migration taking fine-layering into account, *63rd Ann. Int. SEG Mtg,* Expanded Abstr., 653–656. Society of Exploration Geophysicists, Tulsa, OK, USA.

Wapenaar, C.P.A., Slot, R.E. & Hermann, F.J., 1994. Towards an extended macro model, that takes fine-layering into account, *J. Seismic Explor.,* **3,** 245–260.

Widmaier, M.T., Shapiro, S.A. & Hubral, P., 1996. AVO correction for scalar waves in the case of a thinly layered reflector overburden, *Geophysics,* **61,** 520–528.

Zhang, J., Verschuur, D.J. & Wapenaar, C.P.A., 2001. Depth migration of shot records in heterogeneous, transversely isotropic media using optimum explicit operators, *Geophys. Prospect.,* **49,** 287–299.

Zhang, J. & Wapenaar, C.P.A., 2002. Wavefield extrapolation and prestack depth migration in anelastic inhomogeneous media, *Geophys. Prospec.,* **50,** 629–643.